Structural Basis for the Recognition of a Bisphosphorylated MAP Kinase Peptide by Human VHR Protein Phosphatase†

Maria A. Schumacher,* Jacob L. Todd, Adrian E. Rice, Kirk G. Tanner, and John M. Denu*

Department of Biochemistry and Molecular Biology, Oregon Health and Science University, Portland, Oregon 97201-3098

Received September 25, 2001; Revised Manuscript Received January 9, 2002

ABSTRACT: Human VHR (vaccinia H1 related phosphatase) is a member of the dual-specificity phosphatases (DSPs) that often act on bisphosphorylated protein substrates. Unlike most DSPs, VHR displays a strong preference for dephosphorylating phosphotyrosine residues over phosphothreonine residues. Here we describe the 2.75 Å crystal structure of the C124S inactive VHR mutant in complex with a bisphosphorylated peptide corresponding to the MAP kinase activation lip. This structure and subsequent biochemical studies revealed the basis for the strong preference for hydrolyzing phosphotyrosine within bisphosphorylated substrates containing -pTXpY-. In the structure, the two phospho residues are oriented into distinct pockets; the phosphotyrosine is bound in the exposed yet deep active site cleft while the phosphothreonine is loosely tethered into a nearby basic pocket containing Arg^{158}. As this structure is the first substrate−enzyme complex reported for the DSP family of enzymes, these results provide the first glimpse into how DSPs bind their protein substrates.

The specific phosphorylation of tyrosine residues plays a central role in the regulation of cellular functions (*1*). Within the cell, the extent of tyrosine phosphorylation is coordinately regulated by protein tyrosine kinases and phosphatases (*2*). The dual-specificity protein−tyrosine phosphatases (DSPs)[1] are a subfamily of the protein−tyrosine phosphatases (PTPs) (*3*−*6*). To date, over 20 DSPs have been identified (*7*−*10*). Several DSPs have been implicated in MAP kinase regulation by dephosphorylation of both phosphothreonine and phosphotyrosine residues in their TXY motif (where X represents any residue). This dephosphorylation may be a processive mechanism involving a single active site. Phosphorylation of the MAP kinases on both threonine and tyrosine residues leads to dramatic activation and phosphorylation of numerous cellular substrates.

Because it contains only the catalytic domain, the human vaccinia H1 related phosphatase (VHR) has served as the archetypal DSP in biochemical and kinetic studies (*11*, *12*). Initial biochemical studies on VHR revealed that it favors bisphosphorylated substrates over monophosphorylated substrates. In addition, VHR was shown to have weak activity toward phosphothreonine dephosphorylation (*13*, *14*). These data, in addition to the fact that VHR contains conserved sequence motifs found in the DSPs, place it within the DSP family. Like the DSPs, VHR contains the conserved active site sequence HCXXGXXR(S/T); however, outside of this signature region, DSPs show little sequence homology to the PTPs. The invariant cysteine residue in this signature sequence, Cys^{124} in VHR, is essential for catalysis. Indeed, mutation of Cys^{124} to a serine completely abrogates the enzymatic function of VHR (*13*). Recent studies have implicated ERK1 and ERK2 MAP kinases as in vivo substrates for VHR and have revealed that, unlike most DSPs, VHR displays a marked preference for dephosphorylating phosphotyrosine residues (*14*, *15*). Thus, although VHR belongs to the DSP family by virtue of sequence conservation within its catalytic region, its marked preference for dephosphorylating phosphotyrosine residues is interesting and distinguishes it from most DSPs. Therefore, to address the intriguing question of how VHR, like most DSPs, recognizes bisphosphorylated substrates, yet preferentially desphosphorylates phosphotyrosine residues, we determined the crystal structure of the inactive, C124S, mutant of VHR in complex with a bisphosphorylated peptide.

EXPERIMENTAL PROCEDURES

In Vitro Dephosphorylation of p38 by VHR. Active phosphorylated p38 was prepared as described (*16*). VHR (0.4 μM) was incubated with phosphorylated p38 (1.0 μM) at 30 °C for 0−40 min (pH 6.8), and the level of phosphorylated p38 remaining at the indicated times was measured by western blot analysis and quantified using Molecular Analyst. Tyrosine dephosphorylation of DDE(Nle)pTGpY-VATR was followed as the absorbance increase at 282 nm (*14*, *17*). VHR (6 μM) and 1.6 mM peptide were reacted at pH 6 and 25 °C. The progress curve was then fitted to the integrated form of the Michaelis−Menten equation, and the k_{cat}/K_m values were determined from the resulting fits (*14*, *17*).

† M.A.S. is a Burroughs Wellcome Career Development awardee. This work was supported by Grant RPG-97-175-01-TBE (J.M.D.) from the American Cancer Society and by NIH Grant GM59785-02 (J.M.D.).

* To whom correspondence should be addressed. Telephone: (503) 494-2256. Fax: (503) 494-8393. E-mail: schumacm@ohsu.edu or denuj@ohsu.edu.

[1] Abbreviations: DSP, dual-specificity protein−tyrosine phosphatases; PTPs, protein−tyrosine phosphatases; VHR, human *v*accinia *H*1 *r*elated phosphatase; *p*NPP, *p*-nitrophenyl phosphate; MUP, 4-methylumbelliferyl phosphate; 8-FMUP, 8-fluoro-4-methylumbelliferyl phosphate.

10.1021/bi015799l CCC: $22.00
Published on Web 02/08/2002

Mutational Analysis. The R158A and double E126A/Y128I VHR mutants were generated and purified using the same approach as described in ref *18*. The mutations were verified by DNA sequencing. Dephosphorylation on tyrosine was followed as the absorbance increase at 282 nm as described in ref *14*. Dephosphorylation on threonine was measured using a phosphate detection system as we have described previously (*19*). The kinetic parameters were obtained either by fitting progress curves to the integrated form of the Michaelis−Menten equation (*14*, *17*) or by substrate saturation curves and the Michaelis−Menten equation (*14*). Stopped-flow kinetic measurements were performed as described previously (*20*).

Crystallization of the C124S VHR−DDE(Nle)pTGpYVATR Complex. The inactive C124S mutant of VHR was purified as described (*14*) and crystallized with the synthetic bisphosphorylated peptide DDE(Nle)pTGpYVATR. For crystallization, C124S VHR at 5−15 mg mL^{-1} was preincubated with excess peptide (>10 mM), and the complex was mixed 1:1 (v/v) with the reservoir (20% PEG 4000, 10% 2-propanol, 0.1 M citrate, pH = 5.6) and equilibrated against 1 mL of reservoir. The crystals are very small and grow very irreproducibly (only three crystals have been grown). They take the orthorhombic, space group $P2_12_12_1$, with $a = 34.5$ Å, $b = 56.1$ Å, and $c = 101.3$ Å and contain a single VHR−peptide complex in the asymmetric unit.

Structure Determination and Model Refinement. X-ray diffraction data were collected at room temperature at the Stanford Synchrotron Radiation Source using a 180 mm MAR detector and $\lambda = 1.08$ Å. Data were processed with MOSFLM, resulting in an R_{sym} of 9.5%. The data had an $I/(\sigma)I$ for data from 17.3 to 2.75 Å of 17.1. The structure was solved by molecular replacement using the apo VHR structure (*21*) as a search model with MERLOT (*22*). One clear solution was obtained in the rotation function and the subsequent translation function. Cys^{124} of the molecular replacement solution was replaced with a serine (*23*) and the model refined in TNT beginning with xyz followed by xyzb refinement to the limiting resolution of 2.75 Å (*24*). Following initial xyzb refinement, electron density maps revealed weak but clear density for the peptide, which was then modeled (*23*) and refined. The higher temperature factors for the peptide residues and difficulty in obtaining the crystals suggest that the occupancy of the peptide is less than 100% and that the pY is the most tightly anchored of the peptide residues. The final model consists of VHR residues 8−185, 61 water molecules, and all residues (P−6 to P+4) of the peptide. It has an *R*-factor of 18.8% and an R_{free} (calculated using 10% of randomly selected data not used in the refinement) of 26.4% to 2.75 Å resolution (see Table 1). The model, deposited under accession code 1J4X, has rmsd in bond angles and lengths of 0.010 Å and 1.78°. PROCHECK revealed no Ramachadran outliers (*25*).

Table 1: Refinement Statistics

resolution range (Å)	10.0−2.75
no. of reflections	16753
completeness (%)	90
$I/(\sigma)I$ for data from 17.3 to 2.75 Å	17.1
R_{sym}[a]	9.5
R-factor (%)[b]	18.8
R_{free} (%)[c]	26.4
no. of solvent molecules	61
av *B* values (Å^2)	
protein (minus peptide)	17.1
peptide (minus pT and pY)	25.7
pT	24.9
pY	15.0
rms deviations	
bond lengths (Å)	0.010
bond angles (deg)	1.780

[a] $R_{sym} = \sum/I_o - \langle I\rangle/I_o$, where I_o = observed intensity and $\langle I\rangle$ = average intensity obtained from multiple observations of symmetry-related reflections. [b] *R*-factor = $\sum||F_o| - |F_c||/\sum|F_o|$. [c] $R_{free} = \sum||F_o| - |F_c||/\sum|F_o|$, where all reflections belong to a test set of 10% randomly selected data.

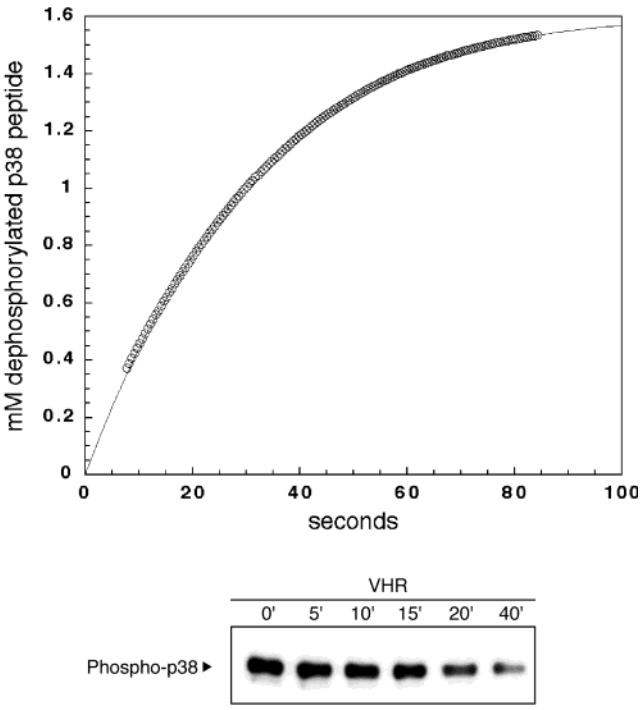

FIGURE 1: In vitro dephosphorylation of p38 MAPK by VHR. (A) Tyrosine dephosphorylation of the bisphosphorylated synthetic peptide DDE(Nle)pTGpYVATR (corresponding to the activation loop of p38 MAPK). Dephosphorylation was followed as the absorbance increase at 282 nm (*14*). VHR (6 μM) and 1.6 mM peptide were reacted in 0.1 M sodium acetate, 0.05 M Bis-Tris, and 0.05 M Tris, pH 6 and 25 °C. The progress curve was then fitted to the integrated Michaelis−Menten equation (*14*) and yielded a k_{cat}/K_m value of 21000 ± 100 M^{-1} s^{-1}. (B) VHR (0.4 μM) was incubated with phosphorylated p38 (1.0 μM) at 30 °C for 0−40 min (pH 6.8), and the level of phosphorylated p38 remaining at the indicated times was measured by western blot analysis. Similar p38 dephosphorylation kinetics were observed from anti-phosphotyrosine western analysis (data not shown). Control experiments without added VHR exhibited no loss of immunoreactivity over the time course of the experiment.

RESULTS AND DISCUSSION

DDE(Nle)pTGpYVATR Is a Substrate for VHR. In an effort to obtain crystals of the catalytically inactive VHR mutant, C124S, in complex with a bisphospho peptide, several bisphosphorylated MAP kinase derived peptides of various sizes and sequences were utilized. Many of these peptides were shown to be substrates of VHR (*14*). Data quality crystals were obtained only with the peptide DDE(Nle)-pTGpYVATR, which is based on the phosphorylation lip of the MAP kinase p38. To evaluate the ability of VHR to dephosphorylate this peptide, dephosphorylation assays were

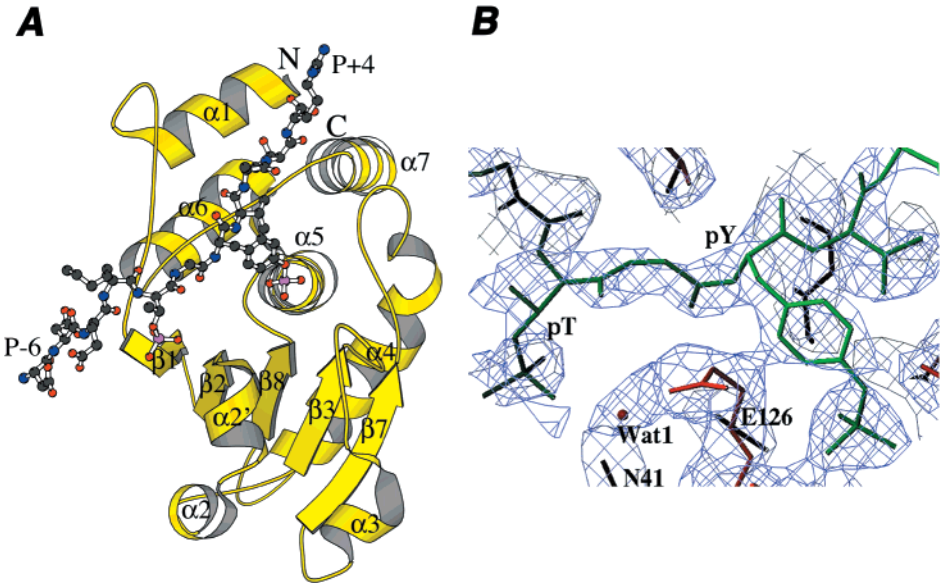

FIGURE 2: Overall C124S VHR−DDE(Nle)pTGpYVATR Complex. (A) Ribbon diagram of the C124S VHR−p38 peptide complex. Secondary structural elements are labeled according to previous convention (*21*). The bound peptide is shown as a ball-and-stick figure with carbon, nitrogen, oxygen, and phosphate atoms colored black, blue, red, and purple, respectively. The peptide is numbered relative to the phosphotyrosine residue (from −6 to +4) such that residues N-terminal to the phosphotyrosine are indicated by negative numbering while residues C-terminal to the phosphotyrosine are indicated by positive numbering. This figure was generated with MOLSCRIPT (*34*). (B) Omit ($F_o - F_c$) electron density map contoured at 3σ and calculated, following convergence of xyzb refinement, with phases from the model in which peptide residues and residues in the phosphoresidue binding sites were omitted. The omit map is shown as a light blue mesh. The peptide is represented as a green stick and the protein as a red stick. Labeled are the phosphotyrosine residue (pY), the phosphothreonine residue (pT), Glu^{126}, Asn^{41}, and the water molecule (Wat1) involved in the phosphothreonine binding site network. The figure was generated in O (*23*).

performed. The phosphotyrosine of this synthetic peptide was rapidly hydrolyzed by VHR, although no significant phosphothreonine hydrolysis was observed over the same time course (Figure 1A). The resulting progress curve was fitted to the integrated Michaelis−Menten equation, yielding a k_{cat}/K_m second-order rate constant of 21000 ± 100 M^{-1} s^{-1}, which is similar to those values determined previously (*14*) for the corresponding bisphosphorylated synthetic peptides of the ERK and JNK MAP kinases.

To demonstrate that VHR could dephosphorylate the intact p38 enzyme in vitro, purified recombinant and phosphorylated p38 protein was reacted with VHR, and the dephosphorylation of p38 was determined by western blot analysis using either an anti-phosphotyrosine antibody (*16*) or an antibody that specifically recognizes bisphosphorylated p38 (Figure 1B). Both western analyses displayed identical dephosphorylation kinetics, again indicating that VHR is rapidly hydrolyzing the phosphotyrosine of active p38 kinase. A k_{cat}/K_m value of 15500 ± 8300 M^{-1} s^{-1} was determined (average of two experiments) for the dephosphorylation of p38 protein by VHR, consistent with the rate measured for the p38 peptide (21000 M^{-1} s^{-1}). A recent report has implicated VHR in regulating the JNK MAP kinase pathway by directly dephosphorylating JNK (*26*). Also, we have determined that the JNK MAP kinase family is an in vivo and in vitro substrate of VHR, in both COS1 and NIH3T3 cells (*36*). Collectively, these previous and current observations suggest that VHR may be a general MAP kinase phosphatase that preferentially hydrolyzes the phosphotyrosine within bis- or monophosphorylated MAP kinases.

Phosphotyrosine Binding and Selective Dephosphorylation. The structure of the VHR(C124S)−DDE(Nle)pTGpYVATR was solved to 2.75 Å and is shown in Figure 2A, and an $F_o - F_c$ omit map of the bisphosphosphorylated peptide binding site is shown in Figure 2B. VHR has a single domain α/β fold with eight α-helices and eight β-strands. In the complex, the peptide binds in an extended conformation through a solvent-exposed crevice created by noncontiguous regions of VHR between α1−α2′, β7−α4, β8−α5, and α6−α7 (Figure 2A). VHR appears to be unique among the DSPs in its marked preference for dephosphorylating phosphotyrosine residues (*15*). Consistent with this preference, the phosphotyrosine residue of peptide, and not the phosphothreonine residue, is bound in the active site cleft of VHR. This pocket is relatively open, and the majority of the contacts made to the phosphotyrosine are to its phosphate moiety, with no stacking interactions to the phosphotyrosine aromatic group (Figure 3A). The phosphate moiety is stabilized by the helix dipole of α5 and hydrogen bonds from the amide nitrogens of residues 125−130 and the side chain of Arg^{130}. The phosphate phosphorus atom is 3.1 Å from the side chain Oγ of Ser^{124}, which would optimally position the wild-type Cys^{124} for nucleophilic attack of the phosphorus atom. This is consistent with biochemical studies demonstrating the formation of the thiol−phosphate intermediate via Cys^{124} in the reaction mechanism (*13*). Also, the tight interaction (Oδ2−O3P, 2.4 Å) observed between the side chain of Asp^{92} and the phenolic oxygen of phosphotyrosine supports the role of Asp^{92} as a general acid/base catalyst (*18*) (Figure 3A).

The lack of specific contacts to the aromatic moiety of the phosphotyrosine as well as the shallower depth of VHR's active site likely explains VHR's weak activity toward dephosphorylating phosphothreonine residues. What, then, is the explanation for VHR's strong preference for phosphotyrosine dephosphorylation? The structure reveals that

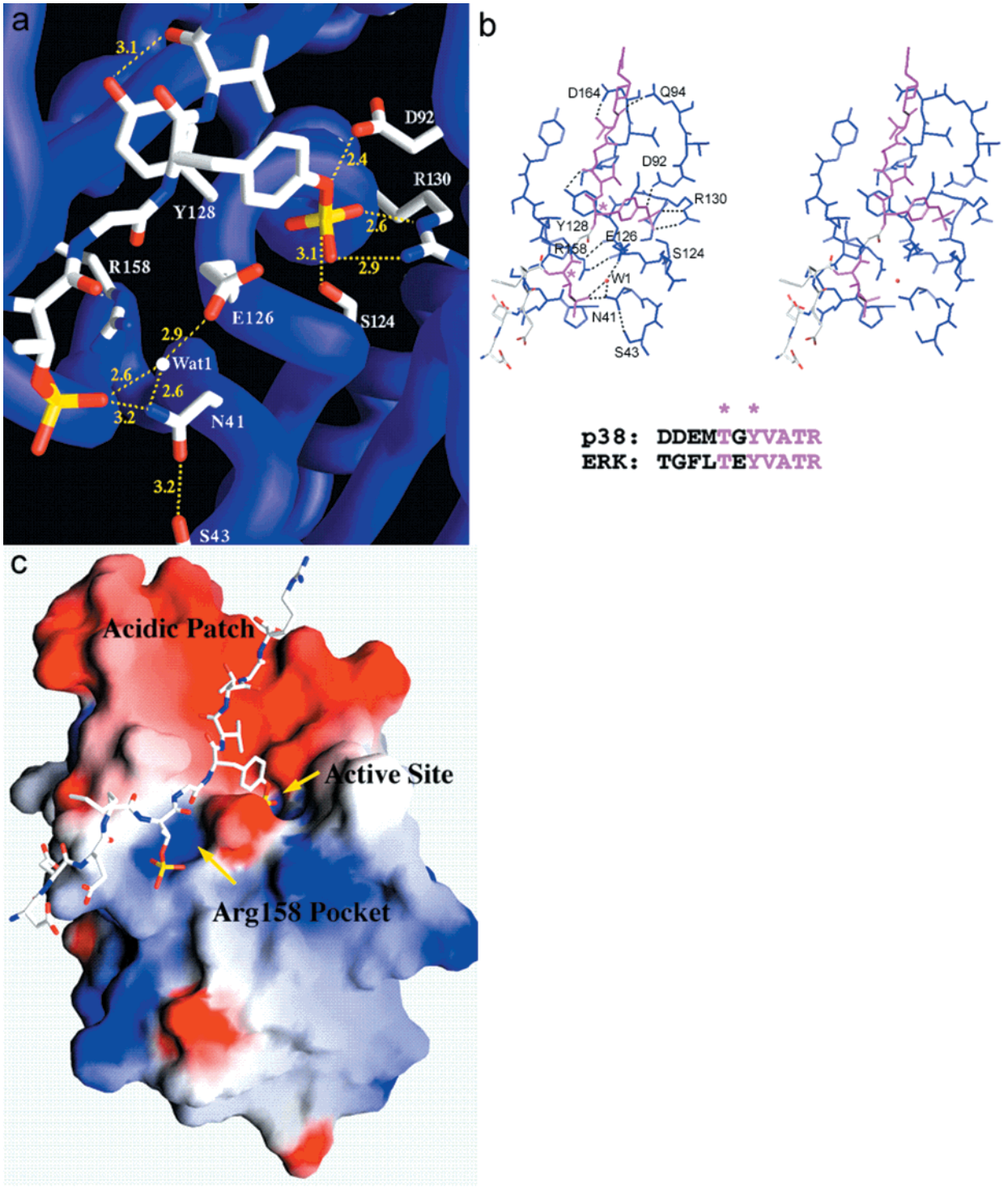

FIGURE 3: C124S VHR−p38 peptide interactions. (A) Close-up of the linked phosphotyrosine and phosphothreonine binding sites. The peptide is shown as a stick with carbon, nitrogen, oxygen, and phosphate atoms colored white, blue, red, and yellow, respectively. This figure was generated with GRASP (*35*). (B) Stereoview of the linked phosphoresidue binding site showing binding of the conserved VATR motif. Residues that are shared in the phosphorylation lip between presumed substrates, p38 and ERK, are colored magenta, and VHR residues are colored blue. The P−2 phosphothreonine and P−1 glycine form a turn that directs the rest of the peptide toward a shallow crevice on the top of VHR. The P+1 valine stacks over VHR residue Tyr^{128}, and its carbonyl makes hydrogen bonds to the Tyr^{128} phenolic oxygen. The P+3 threonine side chain is bound in a pocket formed by Tyr^{23} and the methylene moiety of the Asn^{163} side chain. It also H-bonds via its Oγ to the side chain of Asp^{164}, and its carbonyl oxygen hydrogen bonds, β-strand fashion, to the amide nitrogen of Asp^{164}. In the sequence alignment, the phosphorylated threonine and tyrosine are indicated by asterisks. (C) Electrostatic surface of the VHR−p38 peptide complex. Surfaces are colored according to the local electrostatic potential, ranging from −13 V in dark red and +13 V in dark blue. Notable are the positively charged Arg^{158} phosphothreonine binding pocket and the extensive negatively charged surface near the substrate binding site. The peptide is represented as a stick, and the atoms are colored as in panel a. This figure was generated with GRASP (*35*).

the basis for this discrimination likely lies in the narrow entrance to the active site created by the side chains of Glu^{126} and Tyr^{128}, which are found in the X_2 and X_3 positions of the $HCX_1X_2GX_3X_4R(S/T)$ motif. Tyr^{128} forms the base of

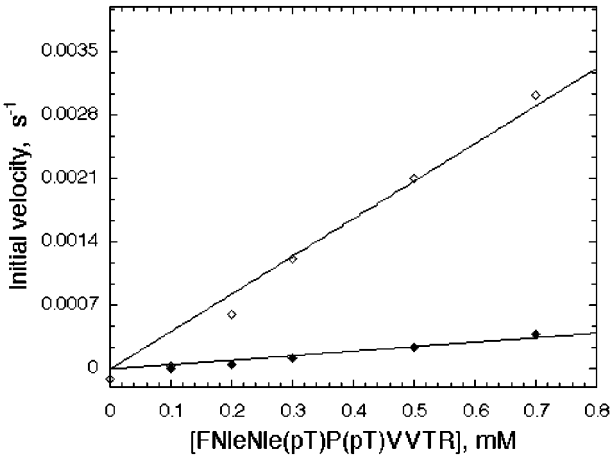

FIGURE 4: Kinetics of FNleNle(pT)P(pT)VVTR peptide dephosphorylation by native and (E126A/Y128I) mutant. Initial rates of dephosphorylation were determined as a function of peptide concentration. Data were fitted to linear least squares regression to obtain the second-order rate constant k_{cat}/K_m. Conditions: 100 mM sodium acetate, 50 mM Bis-Tris, and 50 mM Tris, pH 6 and 30 °C.

the binding site for both the peptide phosphotyrosine and P+1 valine while the aliphatic moiety of Glu[126] provides the only direct contact to the phosphotyrosine ring (Figure 3A,B). Indeed, attempts to dock a phosphothreonine into the active site of VHR, using the position of the phosphotyrosine phosphate as a template, result in steric clash. In contrast to VHR, most DSPs contain the smaller isoleucine and alanine, respectively, instead of tyrosine and glutamic acid at these positions. Smaller residues should allow phosphothreonine binding, thus explaining the greater phosphothreonine dephosphorylation activity of these distinct DSPs.

Therefore, to provide evidence for the role of residues Glu[126] and Tyr[128] in discriminating phosphotyrosine over phosphothreonine, a double mutant (E126A/Y128I) of VHR was created, and the efficiency of hydrolyzing phosphothreonine within the peptide [FNleNle(pT)P(pT)VVTR] was assessed (Figure 4). Ala and Ile were chosen as substitutions because these residues are normally found at the equivalent sites on most DSPs that exhibit greater dual specificity. The phosphopeptide FNleNle(pT)P(pT)VVTR corresponds to the JNK MAP kinases' activation lip, except that the pY has been replaced by a second pT residue. We have previously demonstrated that the phosphotyrosine of the phosphopeptide FNleNle(pT)P(pY)VVTR is hydrolyzed ~1000-fold more efficiently than phosphothreonione (*14*). Here, we compared the ability of native VHR and of the E126A/Y128I mutant to hydrolyze phosphothreonine in FNleNle(pT)P(pT)VVTR (Figure 4). The initial velocities of hydrolysis were determined over a peptide concentration range from 0.1 to 0.7 mM. The k_{cat}/K_m values were determined from the slope of the line. The ability of the E126A/Y128I mutant to hydrolyze phosphothreonine was 9-fold better than for native VHR (4.2 ± 0.2 and 0.49 ± 0.5 M^{-1} s^{-1}, respectively). These findings are consistent with the structural data that suggested that the larger Glu[126] and Tyr[128] residues may participate in restricting pT binding by limiting the depth with which the side chain of pT can access the catalytic nucleophile, Cys[124]. To provide evidence that the increased efficiency for pT dephosphorylation within the peptide substrate is not simply the result of

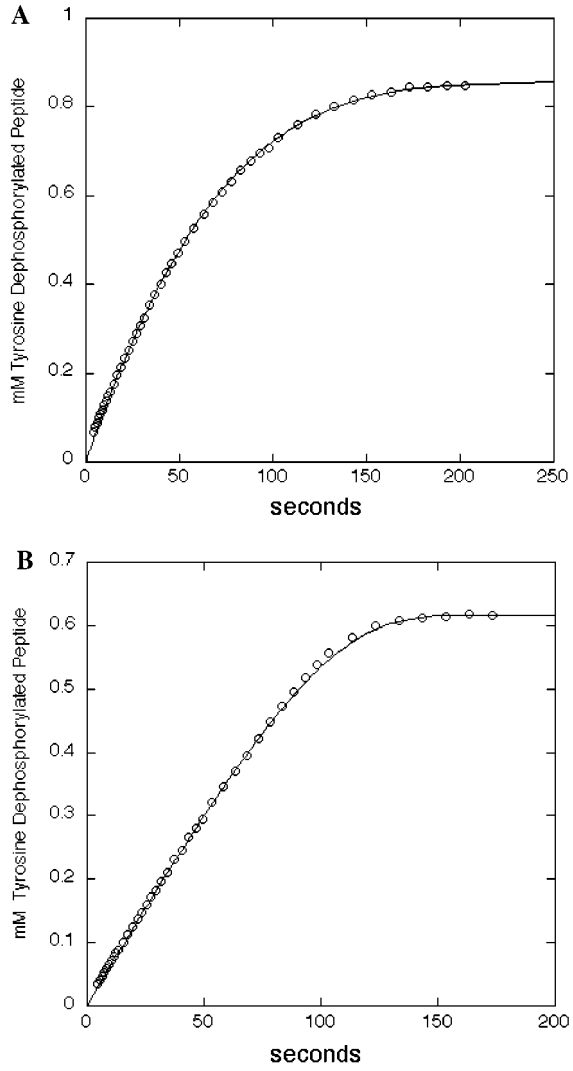

FIGURE 5: Kinetics of FNleNle(pT)P(pY)VVTR peptide tyrosine dephosphorylation by native (A) and (E126A/Y128I) mutant (B). Dephosphorylation was followed as the absorbance increase at 282 nm (*14*, *17*). VHR (3.5 μM) or E126A/Y128I (6 μM) was reacted with 0.48−0.92 mM peptide in 0.1 M sodium acetate, 0.05 M Bis-Tris, and 0.05 M Tris, pH 6 and 25 °C. The progress curve was then fitted to the integrated Michaelis−Menten equation (*14*, *17*). The average of several determinations are listed in Table 2.

a more active enzyme toward peptidic substrates, we examined the ability of the E126A/Y128I mutant to hydrolyze phosphotyrosine in FNleNle(pT)P(pY)VVTR. Phosphotyrosine dephosphorylation was followed spectroscopically and analyzed according to previously described methods (*14*, *17*). The analysis yielded similar k_{cat}/K_m values of 15800 ± 600 and 21500 ± 2300 M^{-1} s^{-1} for VHR and the E126A/Y128I mutant, respectively. Representative data sets are shown in Figure 5. These results indicate that the E126A/Y128I mutant displays similar efficiency (with respect to binding and phospho transfer to the enzyme) for the corresponding pY-containing peptide FNleNle(pT)P(pY)VVTR. Recall that the k_{cat}/K_m value reflects both substrate binding and phospho transfer to the enzyme to form the intermediate (*11*, *12*). Thus, the E126A/Y128I mutant is nearly equivalent to native VHR in its ability to bind this peptide and catalyze the transfer of phosphate from substrate to enzyme. Collectively, these data suggest that Glu[126] and

Table 2: Summary of Kinetic Analysis of E126A/Y128I Mutant of VHR[a]

enzyme	substrate	k_{cat}, s^{-1}	k_{cat}/K_m, M^{-1} s^{-1}	k_{max} of burst, s^{-1}
VHR	8-FMUP	3.80 ± 0.07	1244 ± 90	48.7 ± 3.3
VHR	MUP	4.68 ± 0.13	1418 ± 104	
VHR	*p*NPP	3.74 ± 0.16	230 ± 20	
VHR	FNleNle(pT)P(pY)VVTR	5.56 ± 0.98	15800 ± 600	
VHR	FNleNle(pT)P(pT)VVTR		0.49 ± 0.5	
E126A/Y128I	8-FMUP	0.779 ± 0.008	32200 ± 2000	61.6 ± 4.8
E126A/Y128I	MUP	0.782 ± 0.013	24700 ± 2400	38.4 ± 4.5
E126A/Y128I	*p*NPP	0.81 ± 0.01	2900 ± 100	27.97 ± 2.39
E126A/Y128I	FNleNle(pT)P(pY)VVTR	1.13 ± 0.03	21500 ± 2300	
E126A/Y128I	FNleNle(pT)P(pT)VVTR		4.2 ± 0.2	

[a] The k_{cat} and k_{cat}/K_m values were obtained by fitting initial velocities versus substrate concentrations to the Michaelis−Menten equation. Listed errors are standard errors from the nonlinear least squares fit. Phosphotyrosine dephosphorylation of FNleNle(pT)P(pY)VVTR was followed spectroscopically and analyzed according to previously described methods (*14, 17*). With the phosphotyrosine peptide, kinetic constants were obtained by fitting product progress curves to the integrated form of the Michaelis−Menten equation (*14, 17*). Listed errors are from the standard deviations of two to three experiments using two to three different initial peptide concentrations. The initial velocities of phosphothreonine hydrolysis from FNleNle(pT)P(pT)VVTR were determined over a peptide concentration range from 0.1 to 0.7 mM. The k_{cat}/K_m values were determined from the slope of the line. The k_{max} of the pre-steady-state burst phase was obtained by fitting the $k_{observed}$ as a function of initial substrate concentration to a simple saturation curve (Michaelis−Menten). Each $k_{observed}$ was the average of at least two pre-steady-state kinetic traces. Errors listed for k_{max} are standard errors from the nonlinear least squares fit.

Tyr^{128} may function to restrict the access of pT or pS within protein substrates but do not increase the affinity for pY relative to the substituted residues, Ala and Ile.

To provide further evidence that the E126A/Y128I mutant and native VHR exhibit similar efficiencies of P−O bond cleavage, a detailed steady-state and pre-steady-state kinetic analysis of the E126A/Y128I mutant was performed using a variety of artificial phosphate monoesters as substrates. These substrates [*p*NPP (*p*-nitrophenyl phosphate), MUP (4-methylumbelliferyl phosphate), and 8-FMUP (8-fluoro-4-methylumbelliferyl phosphate)] have been used previously to probe the mechanism of other DSPs (*12, 20*). Steady-state substrate saturation curves were generated, and the data were fitted to the Michaelis−Menten equation. The data for both mutant and native VHR are displayed in Table 2. To obtain the limiting rate of P−O bond cleavage and concomitant phospho transfer to the enzyme, pre-steady-state burst kinetics were analyzed with both enzymes. It has been demonstrated that the limiting rate of P−O bond cleavage can be obtained from burst kinetic measurements, if indeed product bursts are observed (*12*). Previously, it has been difficult to observe burst kinetics with native VHR using the commonly employed substrate *p*NPP (*18*). Burst kinetics can only be observed if the rate of phospho-enzyme intermediate is considerably slower than the rate of phospho-enzyme formation. With *p*NPP and native VHR, these two steps have similar rates. However, when 8-FMUP was used as substrate, clear burst phases were observed in the kinetic traces. This is due to the fact that P−O cleavage is slightly faster with this substrate, whose leaving group pK_a value is lower than *p*NPP (6.4 vs 7.1). The exponential rate of the burst phase was determined as a function of 8-FMUP concentration (Figure 6A). Fitting these data to a simple saturation curve yielded a maximum rate (k_{max}) of 48.7 s^{-1} for P−O cleavage. Burst kinetics were also observed with the E126A/Y128I mutant, yielding a k_{max} of 61.6 s^{-1} (Figure 6B). These comparable rates of P−O cleavage between native and E126A/Y128I enzymes indicate that these enzymes exhibit similar efficiency with respect to the chemistry event of intermediate formation and are consistent with the similar k_{cat}/K_m values for pY dephosphorylation of FNleNle(pT)P(pY)VVTR (see above and Table 2). Although burst kinetics could not be observed using MUP and native VHR, the E126A/Y128I mutant exhibited burst kinetics, yielding a k_{max} value of 38.4 s^{-1}.

The steady-state k_{cat}/K_m value is a measure of both substrate binding and the rate of intermediate formation (*11*). Hydrolysis of the intermediate is not reflected in the k_{cat}/K_m values (*11*). Because P−O cleavage efficiency is largely unaltered in the E126A/Y128I mutant, then it follows that changes in k_{cat}/K_m between native and E126A/Y128I mutant VHR will reflect differences in the efficiencies of substrate binding, as in the case with the FNleNle(pT)P(pT)VVTR peptide. We propose that the 9-fold greater reactivity with the E126A/Y128I mutant for this peptide resulted from a more accessible active site cleft, allowing the pT to protrude toward the catalytic cysteine nucleophile at the bottom of the active site. Consistent with the idea of a more accessible active site, the E126A/Y128I mutant exhibited k_{cat}/K_m values for *p*NPP, MUP, and 8-FMUP that were ∼10−30-fold higher than those obtained with native enzyme (Table 2). The E126A/Y128I mutant displayed turnover values (k_{cat} ∼ 0.8 s^{-1}) that were ∼5-fold lower than those of native enzyme (Table 2). On the basis of the observation of burst kinetics with all phospho monoesters tested, the rate-limiting step for the E126A/Y128I mutant is hydrolysis of the phospho-enzyme intermediate. It is interesting to note that a value of 0.8 s^{-1} is nearly identical to that (0.7 s^{-1}) obtained for the rate of intermediate hydrolysis in the DSP MKP3 (*20*). Native MKP3 efficiently hydrolyzes pT and pY within its substrate and harbors an Ala and an Ile at the equivalent VHR active site positions 126 and 128, respectively. Although it is not clear why MKP3 and the E126A/Y128I mutant of VHR display a slower rate for phospho-enzyme hydrolysis (compared with native VHR), it is possible that these two residues have a small structural role in properly aligning the phosphocysteine for efficient reaction with the attacking water molecule.

Phosphothreonine Recognition Site. Most DSPs bind and react with the bisphosphorylated forms of protein kinases (e.g., MAP kinases and CDK2). VHR displays up to a 2000-fold higher affinity for monophosphorylated tyrosine over monophosphorylated threonine peptides (*14*). Moreover, VHR displays a slight preference (3−8-fold) for bisphopho-

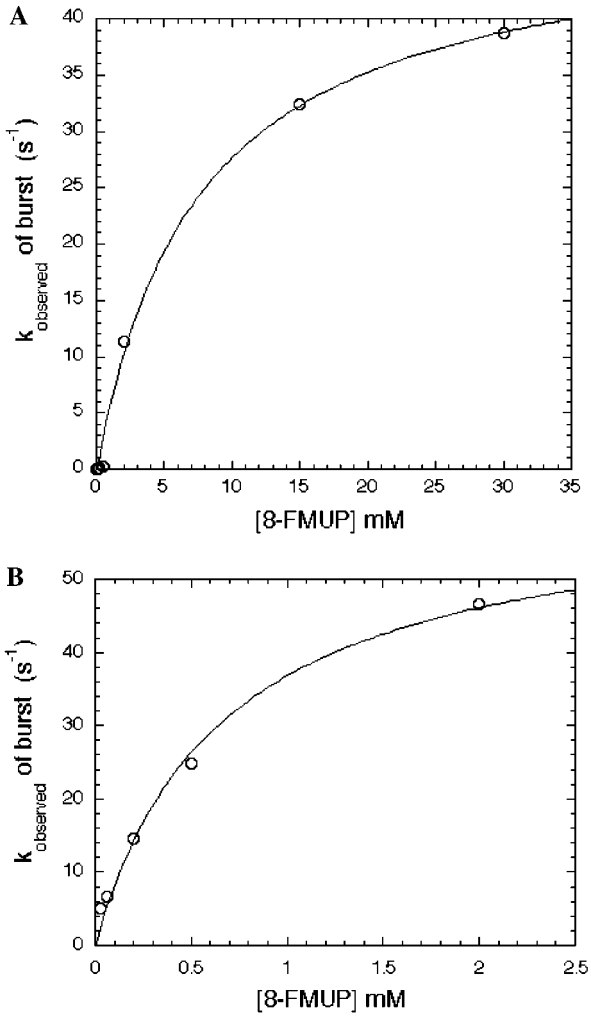

FIGURE 6: Rapid kinetics of VHR (A) and E126A/Y128I mutant (B) reacting with 8-fluoro-4-methylumbelliferyl phosphate. Enzyme (5 μM) and substrate were rapidly reacted in a stopped-flow spectrophotometer, and the formation of product was followed at 359 nm. All kinetic traces displayed an initial burst phase followed by a slower linear phase, which was fitted as previously described (*20*) to obtain the apparent first-order rate constant ($k_{observed}$) of the burst exponential. Each point on the saturation curve is the average of at least two kinetic traces. The substrate concentration dependence of $k_{observed}$ for the burst phase was determined and fitted to the Michaelis−Menten equation. The results are listed in Table 2. Conditions: pH 7 and 25 °C.

phorylated (on tyrosine and threonine) peptides over monophosphorylated tyrosine substrates (*14*).

The structure of the complex, which superimposes onto the apo VHR structure (*21*) with an rms deviation of 0.53 Å for all corresponding Cα residues, reveals that the P−2 phosphothreonine is positioned, via an extensive water-mediated network, into a positively charged pocket formed by Arg[158] (Figure 3C). Specifically, Asn[41], from the N-terminus of α2, and Glu[126], from the catalytic motif, are bridged by a water molecule that forms a hydrogen bond with a phosphate oxygen of the phosphothreonine (Figures 2A and 3A). The Nε of Asn[41] also directly contacts the phosphate moiety. The position of the Asn[41] side chain is further stabilized by a hydrogen bond to Ser[43] (Figure 3A). Interestingly, the phospho residue binding sites in VHR appear to be intimately linked as Glu[126] stacks against the phosphotyrosine phenyl moiety as well as forming part of

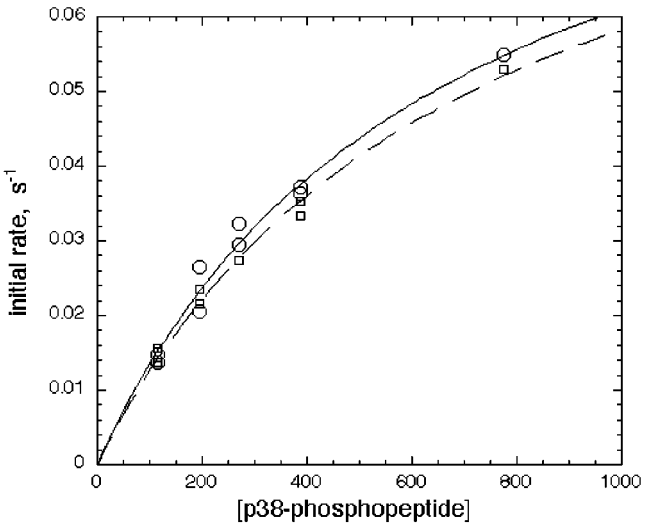

FIGURE 7: Steady-state kinetics of bisphosphorylated DDE(Nle)-pTGpYVATR and monophosphorylated DDE(Nle)TGpYVATR dephosphorylation by R158A VHR mutant. Initial rates of dephosphorylation were determined as a function of peptide concentration. Data were fitted to the Michaelis−Menten equation to obtain the relevant steady-state parameters. Conditions: 100 mM sodium acetate, 50 mM Bis-Tris, and 50 mM Tris, pH 6 and 25 °C.

the phosphothreonine binding water network. Also, Arg[158], in addition to forming the positively charged phosphothreonine binding pocket, provides crucial anchoring hydrogen bonds to the carbonyls of Glu[126] and Gly[27] of the active site pocket (Figure 3A).

Although the position of Arg[158] in the hydrophobic pocket may enhance its positive charge, the side chain of this residue is not within hydrogen-bonding distance to the peptide phosphothreonine (5.4 Å). Therefore, to examine the contribution of Arg[158] to VHR's preference for bisphosphorylated MAP kinase substrates directly, an R158A VHR mutant was generated, and the ability of this mutant to discriminate between bisphosphorylated DDE(Nle)pTGpYVATR and monophosphorylated DDE(Nle)TGpYVATR was determined. Initial rates were determined as a function of peptide concentration and were fitted to the Michaelis−Menten equation (Figure 7). In the R158A mutant, there was no significant difference between the kinetic parameters determined with each peptide. The k_{cat}, K_m, and k_{cat}/K_m values with DDE(Nle)pTGpYVATR were 0.10 ± 0.01 s^{-1}, 653 ± 89 μM, and 155 ± 21 M^{-1} s^{-1} and with DDE(Nle)-TGpYVATR were 0.10 ± 0.01 s^{-1}, 690 ± 80 μM, and 143 ± 16 M^{-1} s^{-1}, respectively. In contrast, the wild-type k_{cat}/K_m values (18900 ± 1430 versus 9840 ± 203 M^{-1} s^{-1}) indicated that native VHR preferred the bisphosphorylated peptide by 2-fold over the monophosphorylated peptide. The 2-fold difference suggests a significant but weak interaction between the pT and Arg[158], consistent with the distance of 5.4 Å observed in the X-ray structure (Figure 3C). Previously, differences of 3−8-fold have been observed with other bisphosphorylated peptides relative to monophosphorylated tyrosine containing peptides (*14*), suggesting that more intimate contact with Arg[158] is possible and may be peptide dependent. The k_{cat} value of wild-type VHR was similar between the bisphosphorylated (4.2 ± 0.6 s^{-1}) and monophosphorylated (5.5 ± 0.5 s^{-1}) peptides, implying that the difference in K_m and k_{cat}/K_m values reflects a change in binding affinity.

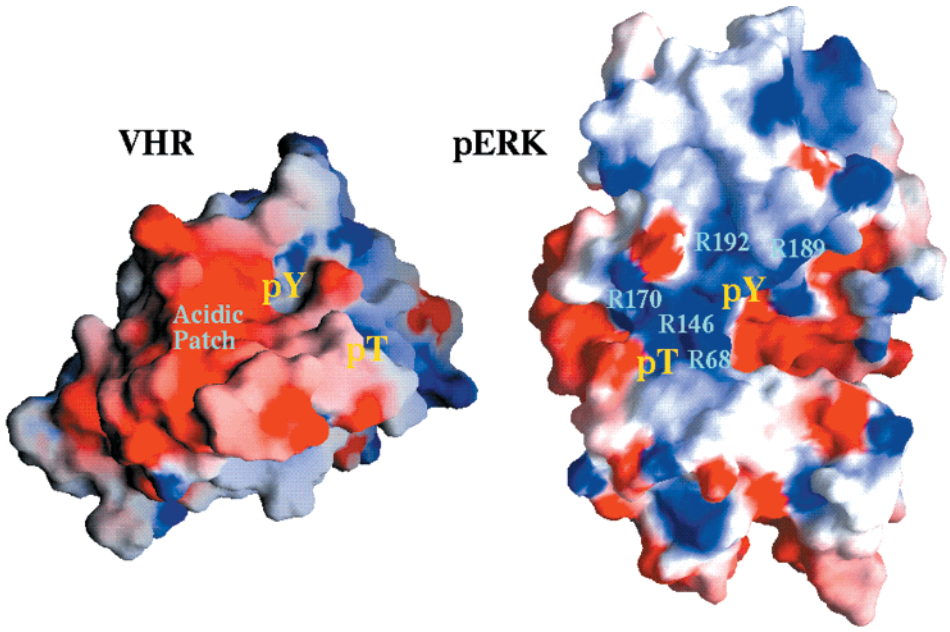

FIGURE 8: Electrostatic surfaces of interacting regions of VHR and its substrate, ERK2. Surfaces are colored as in Figure 3c. Each molecule is rotated to reveal the predicted sites of interaction. The locations of the phosphotyrosine and phosphothreonine residues in pERK2 are indicated by yellow pY and pT labels, and the regions on VHR that interact with these residues are also labeled. Notable is the large negatively charged patch near VHR's substrate binding site that could withdraw the positive residues (indicated in blue) of ERK2 from their sequestering interactions with the phosphoresidues, freeing them for interaction with VHR. This figure was generated with GRASP (*35*).

The main purpose of mutating Arg^{158} was to examine whether this residue had any influence on the binding of the second pT residue in the peptide. This was a logical proposal based on the X-ray structure of VHR complexed to the bisphosphorylated peptide. However, we were completely aware that this Arg is conserved among the PTPs, forming hydrogen bond interactions with the carbonyl oxygens of the active site loop (*12*). So altering this residue would be predicted to decrease the efficiency of the enzyme, independent of its ability to distinguish between bis- versus monophosphorylated peptide substrates. We had hoped that changing this residue would produce an enzyme that still had significant activity so that we could explore substrate preference. Though the mutant is 50−100-fold less efficient in k_{cat} and k_{cat}/K_m parameters for both peptides (k_{cat} = 0.1 s^{-1}) and *p*NPP (0.09 s^{-1}), we were still able to compare whether the R158A mutant showed a significant preference for bis- over monophosphorylated peptide. Moreover, these data are the first to demonstrate biochemical evidence for the structural importance of this Arg in catalysis for PTPs. The lower efficiency of the R158A mutant reaction (namely, the 50−100 fold drop in k_{cat} and k_{cat}/K_m) likely results from the disruption of its stabilizing interaction with the active site pocket (Figure 3A).

Despite relatively low sequence homology, DSPs appear to contain a basic residue corresponding to Arg^{158} in VHR. In addition, the short loop region between α1 and β1, which allows access to the Arg^{158} side chain in VHR, is predicted to be short in all DSPs. However, in other DSPs the presence of an alanine and serine/cysteine at VHR residues Glu^{126} and Asn^{41}, respectively, indicates that a similar anchoring water-mediated network is unlikely in these enzymes. Nonetheless, it is striking that the residue corresponding to Ser^{43} in VHR is either a basic residue (lysine or arginine) or a tyrosine in other DSPs. Arginine, lysine, and tyrosine are the residues most commonly involved in phosphate interactions (*27*). Thus, in other DSPs, these residues may function not only to anchor the P−2 phosphate group into the positively charged pocket but also to provide additional electrostatic interactions with the phosphate group. Since the MAP kinase phosphatases (MKPs) efficiently dephosphorylate both residues of MAP kinase, these stronger interactions may keep the substrate bound for the second round of phospho monoester hydrolysis. Further support that residues corresponding to VHR residues 41−43 are critical for substrate binding in other DSPs comes from recent studies on the DSP Pyst1. Specifically, these studies showed that truncation of residues 207−221 in Pyst1, which correspond to VHR residues 30−44, completely abolishes substrate binding (*28*).

Additional Peptide Contacts and a Suggested Mechanism of Substrate Activation. From the structure it is evident that the phospho residues play the critical role in substrate recognition by VHR. However, additional contacts are provided, primarily, from peptide residues in the P+1 to P+3 positions. The P+1 valine wedges in a pocket where it stacks with the Tyr^{128} ring, while the P+3 threonine side chain Oγ contacts the side chain of Asp^{164} and its carbonyl hydrogen binds with the Asp^{164} amide nitrogen. These residues are also highly conserved in the phosphorylation lips of the MAP kinases, ERK, JNK, and p38 (see Figure 3B). Interestingly, the alanine in the P+2 position sits in a surface-exposed pocket near the side chain of Tyr^{23} such that, in a processive mechanism in which the pT moves to the active site following dephosphorylation of the pY, the dephosphorylated tyrosine could move and make favorable stacking interactions with the Tyr^{23} side chain. Structures available for the nonphosphorylated (inactive) (*29*) and the phosphorylated (active) (*30*) form of VHR's known substrate, ERK2, reveal that the phospho residues of activated ERK2 are sequestered by intramolecular interactions with numerous arginine resi-

dues, presenting an obstacle to VHR binding and catalysis (Figure 8). We postulate that the extensive negatively charged binding surface near the substrate recognition site on VHR could function to ameliorate this obstacle by serving as a negatively charged sink, attracting the arginine side chains, and freeing the phosphotyrosine and phosphothreonine for interaction with VHR (Figure 8).

Comparison to PTPs: An Evolutionary Link. Despite a lack of significant sequence homology, the similarity in structures between the PTPs and the DSPs, as exemplified by PTP1B (*31*−*33*) and VHR (*21*), likely reflects a common evolutionary origin. Perhaps the most divergent region between these proteins corresponds to that between α1 and *β*1. In PTP1B this segment consists of a 41-residue loop−α-helix−loop−*β*-strand−loop structure that helps to form the edge of the deep (10 Å) phosphotyrosine binding pocket. In addition, residues from this area, specifically Tyr^{46}, contribute to phosphotyrosine binding. In VHR, this region is 10 residues long and contains a single loop that creates a shallower active site cleft (6 Å) and exposes the positively charged Arg^{158} pocket that assists in binding the phosphothreonine. Strikingly, this arginine is also conserved in PTPs, likely due to its anchoring role in the catalytic site. However, in PTP1B this residue is completely buried by the inserted region and does not contact its peptide substrate (*32*). In fact, when the two structures are superimposed, the PTP inserted region overlaps the phosphothreonine residue in the VHR−peptide complex. This suggests that many DSPs may have evolved toward recognition of bisphosphorylated substrates through loss of much of the inserted region. Alternatively, the PTPs may have evolved toward the exclusive recognition of a monophosphorylated tyrosine substrate through the addition of the inserted region.

In conclusion, our biochemical and structural studies have demonstrated the basis for VHR's preference for phosphotyrosine dephosphorylation and its preference for bisphosphorylated substrates. Residues shown to be important in these two functions are Glu^{126} and Tyr^{128}, which create a deep, narrow active site that is only easily accessible by phosphotyrosine, and Arg^{158}, which contributes to forming a positive pocket, separate from the active site, for phosphothreonine binding. Finally, the negatively charged patch near VHR's substrate binding site suggests a mechanism for "substrate activation" by releasing the phospho residues that are sequestered around several conserved arginine residues.

REFERENCES

1. Marshall, C. J. (1995) *Cell 80*, 179−185.
2. Hunter, T. (1995) *Cell 80*, 225−236.
3. Tonks, N. K., and Neel, B. (1996) *Cell 87*, 365−368.
4. Fauman, E. B., and Saper, M. A. (1996) *Trends Biochem. Sci. 21*, 413−417.
5. Denu, J. M., Stuckey, J. A., Saper, M. A., and Dixon, J. E. (1996) *Cell 87*, 361−364.
6. Denu, J. M., and Dixon, J. E. (1995) *Proc. Natl. Acad. Sci. U.S.A. 34*, 5910−5914.
7. Guan, K., Broyles, S. S., and Dixon, J. E. (1991) *Nature 350*, 359−362.
8. Kwak, S. P., and Dixon, J. E. (1995) *J. Biol. Chem. 270*, 1156−1160.
9. Groom, L. A., Sneddon, A. A., Alessi, D. R., Dowd, S., and Keyse, S. M. (1996) *EMBO J. 15*, 3621−3632.
10. Keyse, S. M. (1998) *Semin. Cell Dev. Biol. 9*, 143−152.
11. Denu, J. M., and Dixon, J. E. (1998) *Curr. Opin. Chem. Biol. 2*, 633−641.
12. Jackson, M., and Denu, J. D. (2001) *Chem. Rev. 101*, 2313−2340 (2001).
13. Zhou, G., Denu, J. M., Wu, L., and Dixon, J. E. (1994) *J. Biol. Chem. 269*, 28084−28090.
14. Denu, J. M., Zhou, G., Wu, L., Zhao, R, Yuvaniyama, J., and Dixon, J. (1995) *J. Biol. Chem. 270*, 3796−3803.
15. Todd, J. L., Tanner, K. G., and Denu, J. M. (1999) *J. Biol. Chem. 274*, 13271−13280.
16. Khokhlatchev, A., Xu, S., et al. (1997) *J. Biol. Chem. 272*, 11057−11062.
17. Zhang, Z. Y., Maclean, D., Thieme-Sefler, A. M., Roeske, R. W., and Dixon, J. E. (1993) *Anal. Biochem. 211*, 7−15.
18. Denu, J. M., Zhou, G., Guo, Y., and Dixon, J. E. (1995) *Biochemistry 14*, 3396−3403.
19. Fjeld, C. C., and Denu, J. M. (1999) *J. Biol. Chem. 274*, 20336−20343.
20. Fjeld, C. C., Rice, A. E., Kim, Y., Gee, K. R., and Denu, J. M. (2000) *J. Biol. Chem. 275*, 6749−6757.
21. Yuvaniyama, J., Denu, J. M., Dixon, J. E., and Saper, M. A. (1996) *Science 272*, 1328−1331.
22. Fitzgerald, P. M. D. (1988) *J. Appl. Crystallogr. 21*, 273−278.
23. Jones, T. A., Zou, J.- Y., Cowan, S. W., and Kjeldgaard, M. (1991) *Acta Crystallogr. A47*, 110−119.
24. Tronrud, D. E., TenEyck, L. F., and Matthews, B. W. (1985) *Acta Crystallogr. A43*, 489−501.
25. Laskowski, R. A., MacArthur, M. W., and Thorton, J. M. (1993) *J. Appl. Crystallogr. 26*, 283−291.
26. Alonso, A., Saxena, M., Williams, S., and Mustelin, T. (2001) *J. Biol. Chem. 276*, 4766−4771.
27. Copley, R. R., and Barton, G. J. (1994) *J. Mol. Biol. 242*, 321−329.
28. Stewart, A. E., Dowd, S., Keyse, S. M., and McDonald, N. Q. (1998) *Nat. Struct. Biol. 6*, 175−181.
29. Zhang, F., Strand, A., Robbins, D., Cobb, M. H., and Goldmith, E. J. (1994) *Nature 367*, 704−711.
30. Canagarajah, B. J., Khokhlatchev, A., Cobb, M. H., and Goldsmith, E. J. (1997) *Cell 90*, 859−869.
31. Barford, D., Flint, A. J., and Tonks, N. K. (1994) *Science 263*, 1397−1404.
32. Jia, Z., Barford, D., Flint, A. J., and Tonks, M. K. (1995) *Science 268*, 1754−1757.
33. Schubert, H. L., Fauman, E. B., Stuckey, J. A., Dixon, J. E., and Saper, M. A. (1995) *Protein Sci. 4*, 1904−1913.
34. Kraulis, P. J. (1991) *J. Appl. Crystallogr. 24*, 946−950.
35. Nicholls, A., Sharp, K., and Honig, B. H. (1991) *Proteins 11*, 281−296.
36. Todd, J. L., Rigas, J. D., Rafty, L. A., and Denu, J. M. (2002) *Oncogene* (in press).

BI015799L